Structure and Maintenance Process of Stationary Double Snowbands along the Coastal Region

Tadayasu OHIGASHI and Kazuhisa TSUBOKI

Hydrospheric Atmospheric Research Center, Nagoya University, Nagoya, Japan

(Manuscript received 25 June 2004, in final form 22 February 2005)

Abstract

When a cold air outbreak occurred over the Sea of Japan, double snowbands stayed along the coastal region of the Kanazawa Plain from 15 to 16 January 2001: Snowband 1 on the seaward side, and Snowband 2 on the landward side. Their structures are studied mainly using Doppler and dual-polarization radars, and their maintenance processes are discussed. The double snowbands were maintained for about 20 hours. Snowband 1 had a stronger reflectivity and a higher echo top than Snowband 2. The cells in Snowband 2 were generated in the weak echo extending from Snowband 1 toward the land. Around the snowbands, a southeasterly land breeze, with a thickness of 400 m was present. A convergence between the land breeze and the northwesterly monsoon wind formed a strong updraft. Convective cells in Snowband 1 developed in association with the strong updraft. In Snowband 2, a weak convergence produced a weak updraft. The dual-polarization radar data showed that Snowband 1 was composed of spherical graupels, including conical ones. On the other hand, flat-shaped snow crystals were converted to snow aggregates along the trajectory of the particles within Snowband 2. Graupels were seen in the pictures taken below Snowband 1, while only snow aggregates were observed below Snowband 2. These facts indicate that the strong updraft at the land-breeze front contributed to the formation of graupels through the riming process in Snowband 1, on the other hand, snow aggregates developed through the deposition and aggregation processes in the weak updraft in Snowband 2. Some snow crystals, which contributed to the formation of snow aggregates in Snowband 2, were supplied from Snowband 1.

1. Introduction

When outbreaks of winter cold air occur from the Eurasian Continent, snow clouds develop over the Sea of Japan. When snow clouds reach the Japan Islands, they are significantly modified in the coastal region. The modification of snow clouds usually results in the intensification of precipitation. The cause of the intensification is thought to be the topography, contrasts of surface conditions, such as temperature and roughness between land and sea, and local wind in the coastal region. In particular,

the intensification of precipitation occasionally brings a large amount of snowfall to the coastal region. In order to understand heavy snowfall in a coastal region, the modification of snow clouds and the intensification of precipitation in a coastal region must be studied.

Takeda et al. (1982) observed two intensification stages of isolated convective cells of snow clouds in their landing using a radar in Hokuriku. The radar echo of the isolated snow cloud intensified just before landing, and the echo area gradually broadened after landing. Their study did not clarify the kinematical and cloud microphysical processes in the isolated snow cloud, because neither Doppler nor polarization properties were available.

Some previous studies using an aircraft and Doppler radars have shown that a land breeze

Corresponding author: Tadayasu Ohigashi, Hydrospheric Atmospheric Research Center, Nagoya University, Nagoya, 464-8601 Japan.
E-mail: ohigashi@rain.hyarc.nagoya-u.ac.jp

plays an important role in the intensification of snowfall. Passarelli and Braham (1981) observed shoreline-parallel snowbands, which developed over Lake Michigan of the Great Lakes, using an aircraft and a radar. The aircraft observation showed that land breezes, with a thickness of a few hundred meters, developed and made a strong convergence with the ambient flow in the low level over the lake. Snowbands echo developed around the land-breeze front with the low-level strong convergence. Ishihara et al. (1989) revealed that a land breeze developed when the wind speed of the winter monsoon was relatively weak, and moderately cold air was located in the middle and lower troposphere. They also studied the structure of snowbands associated with a land breeze using a Doppler radar in Hokuriku. The snowbands moved toward the land with the retreat of the land-breeze front and decayed after its landing. Then, the land-breeze front extended toward the sea, and another snowband developed along the front. Fujiyoshi et al. (1988) and Tsuboki et al. (1989a) studied snow clouds, which rapidly developed at land-breeze fronts along the west coast of Hokkaido, using a Doppler radar. They observed two different types of snowbands. The snowband studied by Fujiyoshi et al. (1988) moved toward the land, and a weak updraft was present above the land-breeze layer behind the front. On the other hand, the snowband studied by Tsuboki et al. (1989a) moved toward the sea, and a distinct subsidence was present behind the front. Tsuboki et al. (1989b) reported that snowband echoes continuously intensified at a stationary land-breeze front when the snowband intruded into a plain. The echoes intensified at the land-breeze front and rapidly disappeared behind the front. The intensification brought localized heavy snowfall in the coastal region.

Cloud microphysical properties should be investigated to understand the intensification of snowfall in the coastal region. The solid precipitation particles grow through the processes of deposition, riming, and aggregation. Harimaya and Sato (1992) examined the contribution of the riming process to the snowfall amount in the west coast of Hokkaido by surface and radar observations. They clarified that the riming process is predominant in snowfall in the coastal region. They also showed that the riming process brings strong snowfalls and is predominant during the developing and mature stages of snow clouds. Moreover, Harimaya and Kanemura (1995) clarified, using a Doppler radar and surface observations, that the riming process is predominant when updrafts are strong in the clouds, and that developing or mature stages of snow clouds appear more frequently in the coastal region than in the inland region. Namely, most snowfall in the coastal region is brought by the riming process associated with strong updrafts in developing or mature stages of snow clouds, which frequently appear in the coastal region. The microphysical aspects of clouds in the studies were discussed from surface observation alone. Therefore, the relationship between the intensification of snowfall, and cloud microphysical processes in clouds, remains to be studied.

In order to understand the intensification of snowfall in coastal regions, both kinematical and cloud microphysical processes in snow clouds should be observed simultaneously. However, there were no such observations with respect to snow clouds in coastal regions, and only a few studies have focused on a modification of snow clouds so far.

An intensive observation of snowstorms was carried out from November 2000 to February 2001 in Hokuriku using the Doppler radar of Nagoya University. During the observation period, double snowbands stayed along the coastal region for about 20 hours and brought a large amount of snowfall to the coastal region of Hokuriku. In this study, the kinematical and cloud microphysical structures of the stationary double snowbands along the coastal region are investigated, mostly with the use of Doppler and dual-polarization radars. In addition, the maintenance processes of the stationary double snowbands are discussed, to clarify the intensification processes of snowfall in the coastal region.

2. Observation and data

The X-band Doppler radar of Nagoya University was installed at Oshimizu in Hokuriku, Japan (Fig. 1) from 24 December 2000 to 12 February 2001 as a part of the special observation of the "Winter Mesoscale Convective Systems Observation over the Japan Sea 2001 (WMO-01)" (Yoshizaki et al. 2001). Hereafter,
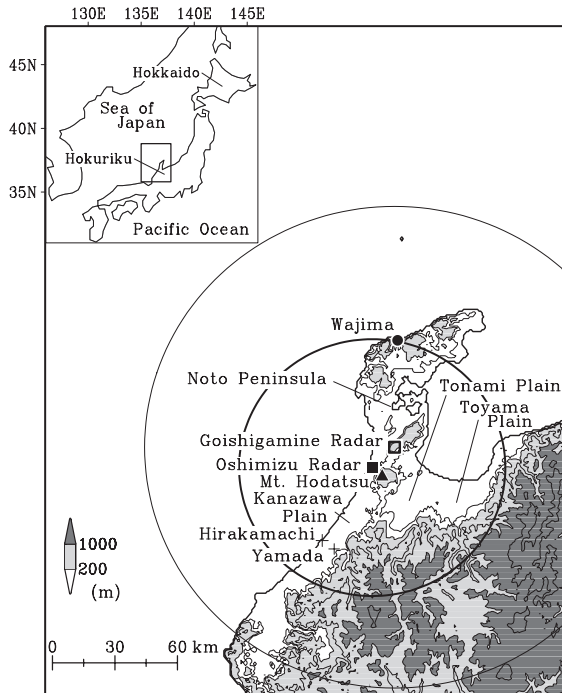
Fig. 1. Locations of observation points. ■ and □ indicate the observation points of the X-band Doppler radar of Nagoya University installed at Oshimizu and the C-band dual-polarization radar of the Hokuriku Electric Power Company set at Goishigamine, respectively. The thick and thin circles indicate their observation ranges. The upper-air sounding observation site at Wajima is marked with ●. Pictures of snow particles were taken at Hirakamachi and Yamada marked with +. The altitude of the topography is shown with contours and gray levels. The contours are drawn at 0, 100, 200, 500, 1000, and 2000 m.

Table 1. Characteristics of the Doppler radar of Nagoya University.

Transmitting frequency	9375 MHz (X-band)
Peak transmitting power	40 kW
Pulse length	0.5 μ sec
Pulse repetition frequency	2000 Hz
Beam width	1.2°
Range gate width	250 m
Maximum range of data processing	64 km
Nyquist velocity	16 m s^{-1}
Doppler processing	Pulse-pair processing

Table 2. Characteristics of the dual-polarization radar of the Hokuriku Electric Power Company.

Transmitting frequency	5320 MHz (C-band)
Peak transmitting power	250 kW
Pulse length	0.8 μ sec
Pulse repetition frequency	1180 Hz
Beam width	1.0°
Range gate width	250 m
Maximum range of data processing	120 km

the radar is referred to as the "Oshimizu radar." Table 1 summarizes its characteristics. The Oshimizu radar was operated with 11 Plan Position Indicator (PPI) scans, and one Range Height Indicator (RHI) scan in 6 minutes to obtain the equivalent reflectivity factor (Z_e) and the Doppler velocity (V_R). The elevation angles of the PPI scans were 0.6, 1.2, 1.9, 2.8, 3.9, 5.1, 6.8, 9.1, 12.3, 17.0, and 25.0 degrees. The C-band dual-polarization Doppler radar is located at Goishigamine (Fig. 1). The radar, which is hereafter referred to as the "Goishig-

amine radar," is used for routine observations by the Hokuriku Electric Power Company to obtain the Z_e, V_R, spectrum width, and differential reflectivity factor (Z_{DR}). In this study, Z_e and Z_{DR} were used. The characteristics of the Goishigamine radar are shown in Table 2. The definition of Z_{DR} is

$$Z_{DR} = 10 \log_{10}\left(\frac{Z_{HH}}{Z_{VV}}\right), \quad (1)$$

where Z_{HH} and Z_{VV} are the horizontally transmitted/horizontally received and vertically transmitted/vertically received reflectivity factors, respectively (Seliga and Bringi 1976). A horizontally oriented particle has a positive Z_{DR}, and a vertically oriented particle has a negative Z_{DR}. A completely spherical particle has a Z_{DR} of 0 dB. The Goishigamine radar was operated in 5 minutes with 13 PPI scans, which have elevation angles of −0.4, 0.1, 0.6, 1.1, 1.6, 2.1, 3.1, 4.1, 6.1, 9.1, 12.1, 20.0, and 30.1 degrees.

The regional objective analysis (RANAL) data, the upper-air sounding data at Wajima (Fig. 1) provided by the Japan Meteorological Agency (JMA), and the NOAA satellite data

received at the Hydrospheric Atmospheric Research Center of Nagoya University were used to examine the synoptic situation and cloud distribution. The air temperature at the sea level was calculated using the dry adiabatic lapse rate from the air temperature at the surface of the RANAL data. Surface wind data, obtained by the Automated Meteorological Data Acquisition System (AMeDAS) of the JMA, was employed in examining the meso-scale environmental features around the snow-bands. In addition, pictures of snow particles were utilized. The pictures of snow particles were taken by digital cameras after snow particles were captured on wood boards covered with a velvet cloth at Hirakamachi and Yamada (Fig. 1), in order to investigate the cloud microphysical characteristics of snowfall particles near the coast by observation members of Nagoya University.

The Z_e, V_R, and Z_{DR} obtained from the radars were interpolated on the Cartesian coordinate system with horizontal intervals of 0.5 km and vertical intervals of 0.25 km (Constant Altitude Plan Position Indicator [CAPPI] data). A correction of radar-echo advection was applied (Gal-Chen 1982). The Velocity-Azimuth Display (VAD) method (Tsuboki and Wakahama 1988) was used to determine a wind field above the Oshimizu radar on the vertical coordinate with intervals of 50 m. Using RHI data obtained by the Oshimizu radar, the horizontal velocities (V_H) were derived from

$$V_H = \frac{V_R}{\cos \alpha}, \qquad (2)$$

where α is an elevation angle. RHI data with elevation angles of less than $30°$ was used for maintaining accuracy. Furthermore, a horizontal divergence was calculated from the horizontal wind derived from the RHI data assuming no divergence in the direction normal to the RHI scan.

Although the equivalent reflectivity factor (Z_e) is derived from radar, the reflectivity factor (Z), instead of Z_e, is used hereafter for simplicity.

3. Synoptic situation

The synoptic charts of RANAL data at the surface and 500 hPa at 21 JST (Japan Standard Time) on 15 January 2001 are shown in
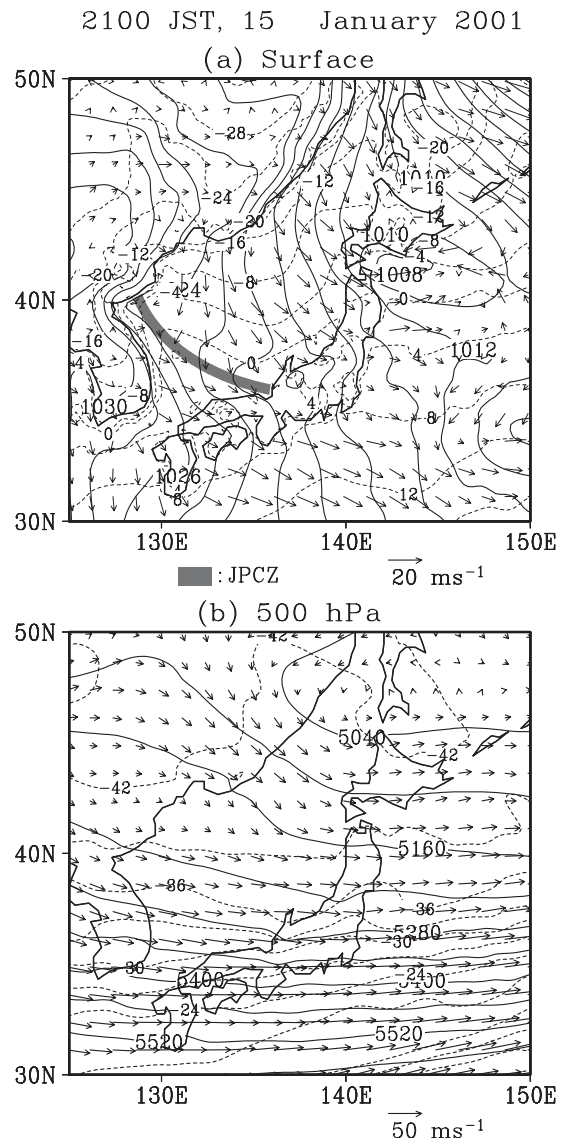
2100 JST, 15   January 2001

Fig. 2.   (a) Sea-level pressure (solid lines, hPa), sea-level temperature (dashed lines, °C), and surface wind field (arrows), and (b) geopotential height (solid lines, m), temperature (dashed lines, °C), and horizontal wind field (arrows) at 500 hPa at 21 JST, 15 January 2001 of the regional objective analysis (RANAL) data. The shaded area in (a) represents the Japan-Sea Polar-airmass Convergence Zone (JPCZ).

Fig. 2. On the surface, the isotherms cross the isobars over the Sea of Japan, and the northerly or northwesterly wind caused cold advection from the Eurasian Continent to the
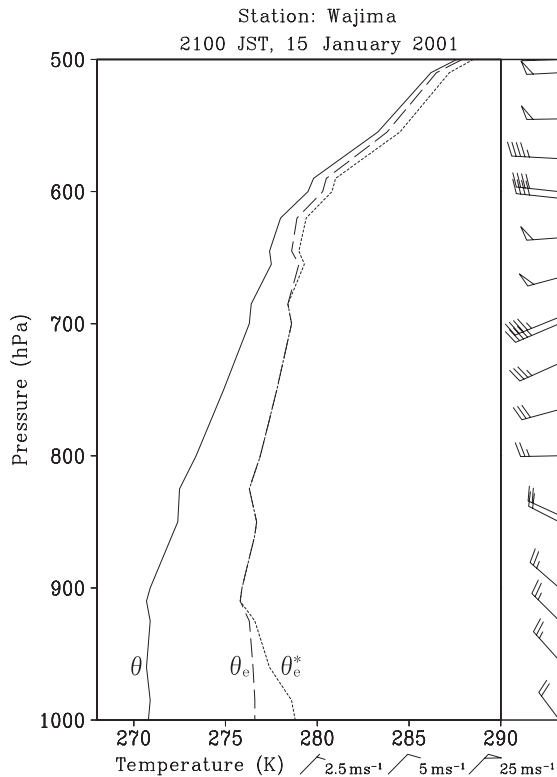
Station: Wajima
2100 JST, 15 January 2001

Fig. 3. Vertical profiles of the potential temperature (θ), equivalent potential temperature (θ_e), saturated equivalent potential temperature (θ_e^*), and horizontal wind at 21 JST, 15 January 2001 at Wajima. A half barb, a full barb, and a flag indicate 2.5 m s^{-1}, 5 m s^{-1}, and 25 m s^{-1}, respectively.

Fig. 4. NOAA-14 channel 4 (thermal-infrared) satellite image at 1523 JST, 15 January 2001.

Sea of Japan. In the southwest region of the Sea of Japan, a convergence zone was formed to the east of the Korean Peninsula. The convergence zone is referred to as the Japan-Sea Polar-airmass Convergence Zone (JPCZ) (Asai 1988). At 500 hPa, cold air less than $-33°C$ was present over Hokuriku. The counterclockwise turning of the wind direction from N or NW at the surface, to WNW at 500 hPa over the western Sea of Japan, indicates cold advection.

The relatively warm sea supplies sensible heat and latent heat to the cold air, and a mixing layer develops over the sea. At 21 JST, 15 January 2001 at Wajima, the potential temperature (θ) shows that the mixing layer was present below 600 hPa (Fig. 3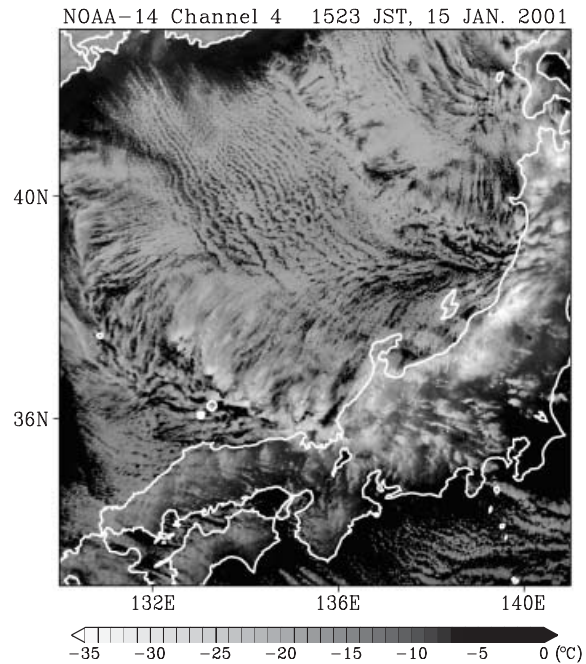). The small difference between the equivalent potential temperature (θ_e), and the saturated equivalent potential temperature (θ_e^*), indicates that the atmosphere in the mixing layer was almost saturated except for the lowest level and the uppermost part of the mixing layer. The counterclockwise turning of the wind direction from NW near the surface to WSW at 700 hPa indicates cold advection. The wind speed in the lower level was not too strong (less than 12 m s^{-1} below 800 hPa). The weak static stability in the mixing layer, and the relatively weak wind in the lower level, are favorable conditions for the development of a land breeze.

Many cloud streaks developed in the mixing layer (Fig. 4). A cumulonimbus cloud line with a high cloud top (a height of about 650 hPa), which was located along the JPCZ shown in Fig. 2a, extended from NW to SE in the western part of the Sea of Japan. Another type of cloud lines, with an alignment from SW to NE, extended from the active cumulonimbus line along the JPCZ. The alignment of SW to NE was almost perpendicular to the northwesterly wind in the lower troposphere in the sounding profile at Wajima. The cloud lines that are almost perpendicular to the wind are
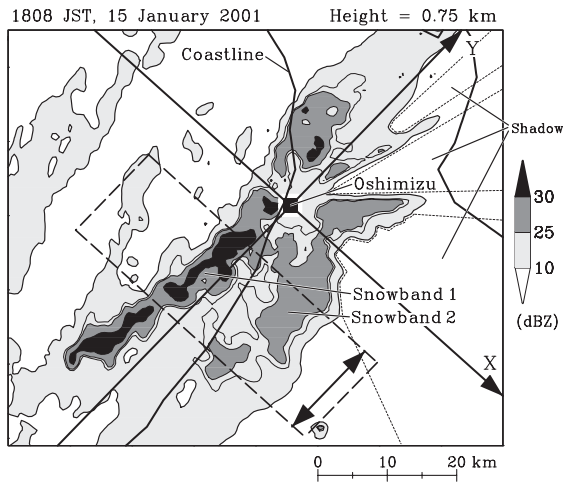
Fig. 5. CAPPI display of the reflectivity at 1808 JST, 15 January 2001 at a height of 0.75 km. The contours are drawn at 10, 23, 25, and 30 dBZ. ■ indicates the location of the Oshimizu radar. The solid lines with an arrow show the X and Y axes. The rectangle with broken lines corresponds to the averaged area in Figs. 6, 8, and 16b.

referred to as "transverse-mode cloud bands." The snowbands investigated in detail in this study stayed along the coastal region (around 136.5°E and 36.5°N), where the transverse-mode cloud bands landed. In the lower level of the region of transverse-mode cloud bands, the wind speed was weaker than in other regions where there were outbreaks of cold air. Furthermore, the pressure gradient in the lower level was small in the region of transverse-mode cloud bands, especially near the coastal region of Hokuriku (Fig. 2a). This is a favorable situation for a land breeze to develop.

4. Structure of snowbands

4.1 Echo structure

Figure 5 shows a representative display of double snowbands. The double snowbands were present along the coastal region of the Kanazawa Plain in Hokuriku, which are referred to as "Snowband 1" and "Snowband 2." The snowbands stayed at almost the same position with almost the same alignment. These snowbands along the coastal region are investigated in detail. The X and Y axes are defined normal and

parallel to the alignment of the snowbands, respectively, as shown in Fig. 5.

A time-distance cross section at a height of 0.75 km shows the time evolution of the double snowbands (Fig. 6). The reflectivity was averaged from $Y = -24$ km to -8 km (in the rectangle area of Fig. 5) in the Y-direction. The averaged range was selected to exclude shadow regions due to topography. The double snowbands were present between $X = -10$ km and 20 km during the period from 0730 JST, 15 to 0400 JST, 16 January 2001. Snowbands 1 and 2 were located around $X = -3$ km to 2 km and $X = 9$ km to 13 km, respectively. The snowbands had different features before and after 1500 JST, 15 January 2001. After 1500 JST, Snowband 2 possessed relatively weak reflectivity, and the separation of the double bands was clear. The present study focuses on the double snowbands from 1500 JST, 15 to 0400 JST, 16 January 2001. This period is referred to as the "period of double bands." Almost no echo merged into the double bands in the period of double bands, while the transverse-mode cloud bands were present in the upwind side of the double bands (shown in Fig. 4). Therefore, the updraft in the transverse-mode cloud bands was weak. This indicates that the circulation that formed around the coastal region, in which the double bands stayed, was essential for the formation of the double bands.

A horizontal display of time-averaged reflectivity at a height of 0.75 km (Fig. 7) shows that Snowband 1 extended from the sea to the land, and that its reflectivity was relatively strong (more than 26 dBZ). Snowband 2 was located over the land, and its reflectivity was relatively weak (less than 26 dBZ). The widths of both snowbands defined by the contour of 23 dBZ ranged from 5 to 8 km.

The vertical cross section of reflectivity (Fig. 8), which was averaged from $Y = -24$ km to -8 km (in the rectangle area in Fig. 5) in the Y-direction, also shows Snowband 1 with strong reflectivity and Snowband 2 with weak reflectivity. Snowband 1 has a higher echo top reaching a height of 2.5 km when the echo top was defined by a contour of 10 dBZ. The echo top of Snowband 1 significantly decreased toward the landward side. The axis of Snowband 1 leaned to the seaward side with height.
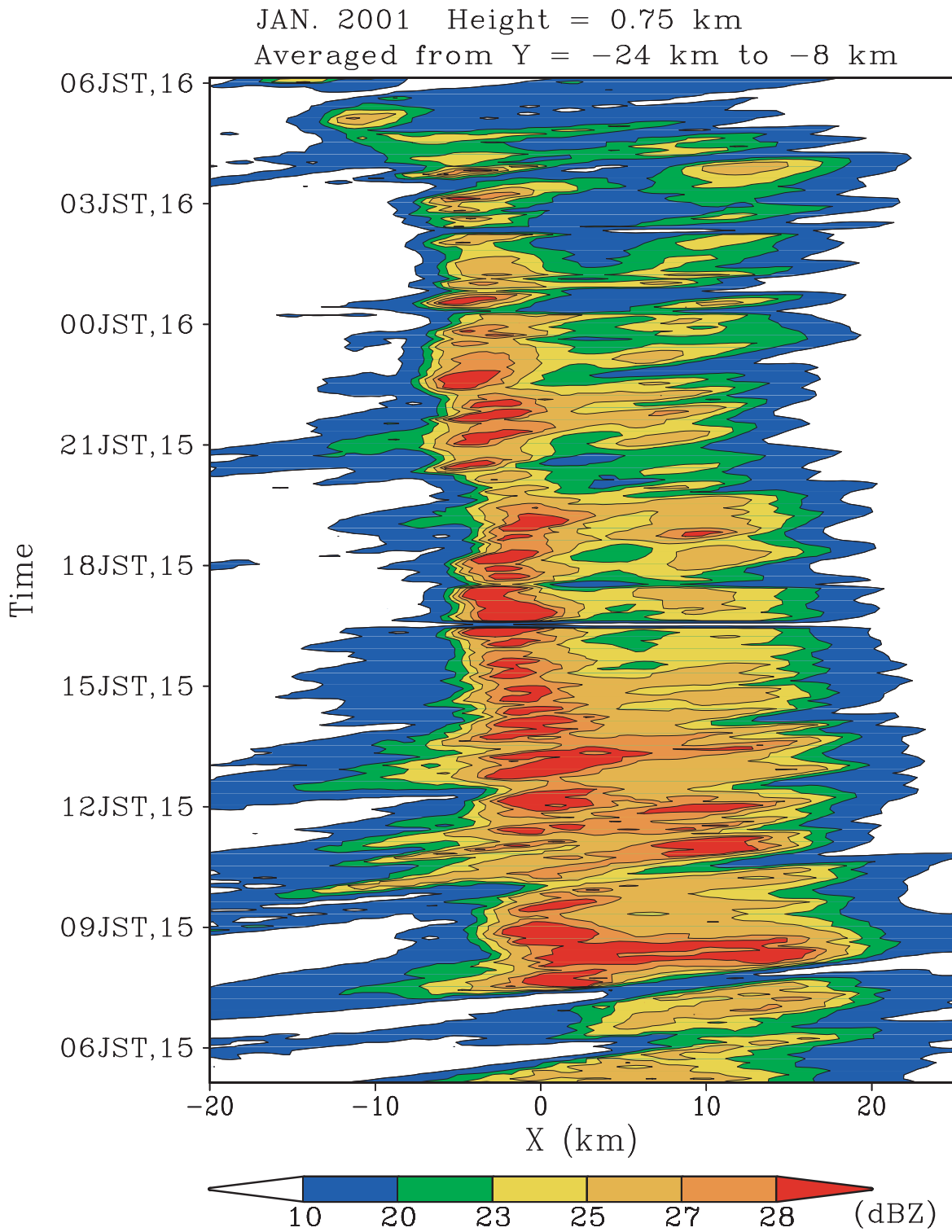
Fig. 6. Time-distance cross section of the reflectivity at a height of 0.75 km. The reflectivity is averaged from Y = −24 km to −8 km in the Y-direction (the rectangle area with broken lines in Fig. 5).

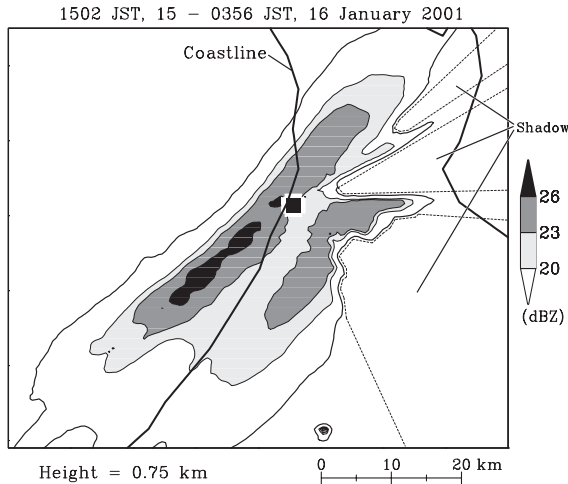1502 JST, 15 − 0356 JST, 16 January 2001

Fig. 7. CAPPI display of the time-averaged reflectivity from 1502 JST, 15 to 0356 JST, 16 January 2001 at a height of 0.75 km. The contours are drawn at 10, 20, 23, and 26 dBZ.
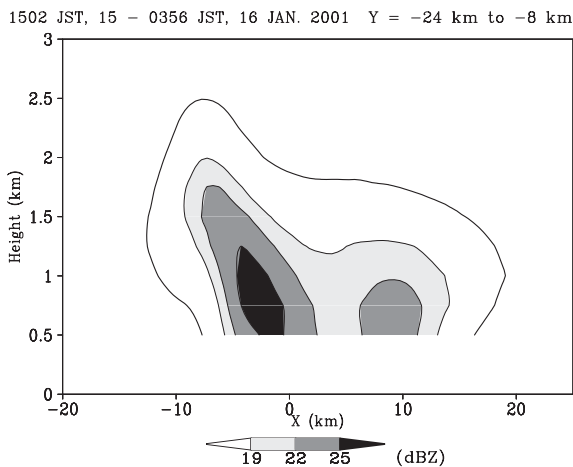
1502 JST, 15 − 0356 JST, 16 JAN. 2001 Y = −24 km to −8 km

Fig. 8. Vertical cross section of the time-averaged reflectivity from 1502 JST, 15 to 0356 JST, 16 January 2001. The reflectivity is also averaged from $Y = -24$ km to -8 km in the Y-direction (the rectangle area with broken lines in Fig. 5). The contours are drawn at 10, 19, 22, and 25 dBZ.

Snowband 2 had a lower echo top than Snowband 1, with a height of 1.75 km, and a contour of 10 dBZ protruded inland. The reflectivity between Snowband 1 and Snowband 2 showed a minimum.

In order to examine the maintenance process of both bands, the development and movement of the cells are investigated. Figure 9 shows a time-series of radar echoes every 6 minutes from 2056 JST to 2202 JST, 15 January 2001 during the period of double bands. Each snapshot was averaged from $Y = -13$ km to -8 km in the Y-direction to clarify the characteristics of cellular echoes. A new cell of Snowband 1 with 26 dBZ was generated at $X = -9$ km, and a height of 1.75 km at 2102 JST, and is named SB1-1. SB1-1 rapidly developed between 2102 JST and 2114 JST to have stronger reflectivity than 28 dBZ while moving inland. Then, SB1-1 descended without intensifying after 2120 JST. New cells of Snowband 1 developed at 2126 JST (SB1-2) and at 2150 JST (SB1-3). These cells (SB1-2 and SB1-3) behaved in the same manner as SB1-1.

A cell (SB2-1) of Snowband 2 with 24 dBZ was generated at $X = 4$ km and at a height of 1 km at 2126 JST. At the same time, the echo top with 10 dBZ over SB2-1 slightly ascended, while the echo top between SB1-2 of Snowband 1 and SB2-1 of Snowband 2 descended ($X = -5$ km). After 2132 JST, SB2-1 slowly intensified and descended. The echo top between SB1-2 of Snowband 1 and SB2-1 of Snowband 2 further descended. The axis of SB2-1 inclined inland with time. Another cell (SB2-2) of Snowband 2 appeared at 2156 JST. Cell SB2-2 followed a similar evolution to SB2-1.

The cells of Snowband 1 intensified more rapidly and had stronger reflectivity than those of Snowband 2. The echo top (10 dBZ) of Snowband 1 was higher than that of Snowband 2. The inclinations of the cells of both bands were different from each other. It should be noted that the cells of Snowband 2 were generated at the positions where the weak echo regions of Snowband 1 extended inland. This suggests that the formation of cells of Snowband 2 is related to Snowband 1.

4.2 Kinematical structure

The structure of the airflow around the snowbands is described to show the kinematical aspects of maintenance processes of the snowbands. Figure 10 shows the time-height cross section of the horizontal wind above the Oshimizu radar obtained by the VAD method. The contours indicate the X-component of the

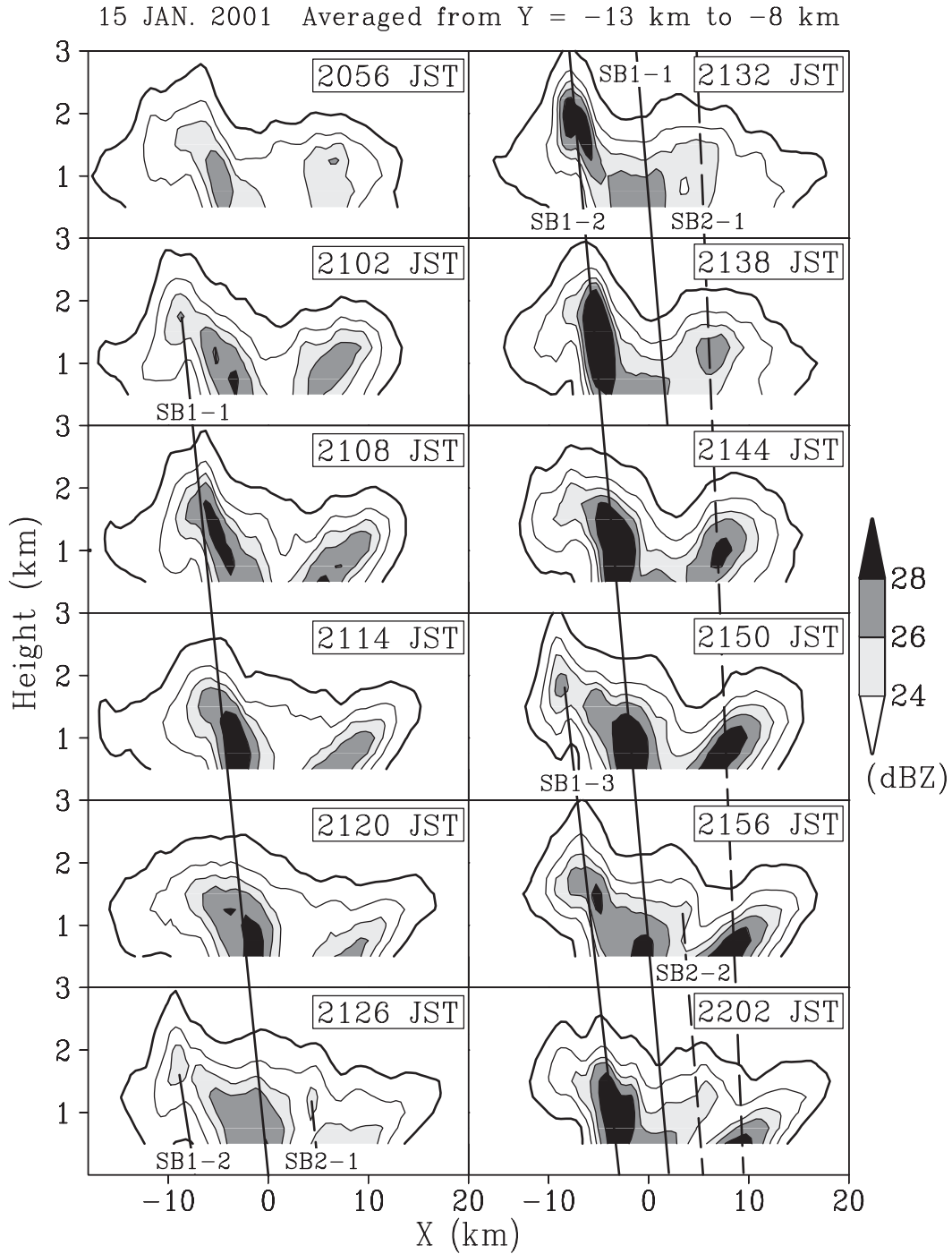15 JAN. 2001   Averaged from Y = −13 km to −8 km

Fig. 9.   Time-series of vertical cross sections of the reflectivity every 6 minutes from 2056 JST to 2202 JST, 15 January 2001. The reflectivity is averaged from −13 km to −8 km in the Y-direction. The contours are drawn at 10, 20, 24, 26, and 28 dBZ. Thick solid lines and thick broken lines follow the movements of cells.
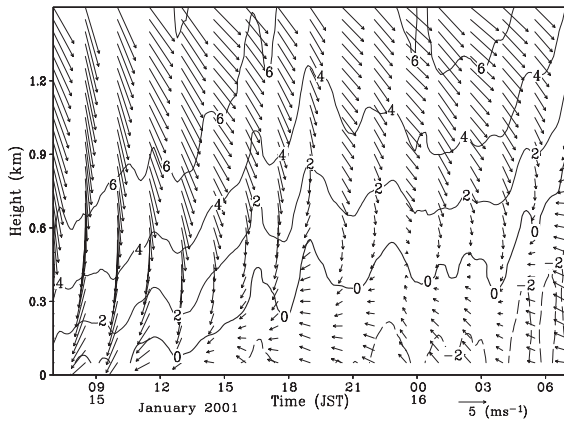
Fig. 10. Time-height cross section of the horizontal wind above the Oshimizu radar obtained by the VAD method. The contours indicate the X-component of wind speed every 2 m s^{-1} on the X and Y coordinate system defined in Fig. 5.

Fig. 11. Surface wind at AMeDAS points at 2100 JST, 15 January 2001. Double open circles represent calm. A half barb and a full barb show 1 m s^{-1} and 2 m s^{-1}, respectively. The altitude of the topography is shown with contours and gray levels. The contours are drawn at 0, 100, 200, 500, 1000, and 2000 m.

horizontal wind on the X and Y axes defined in Fig. 5, where the positive values represent wind from the sea to the land. At a height of 1 km, the northwesterly monsoon wind prevailed. Its direction was almost constant with time, while the X-component of the horizontal wind gradually decreased until 1630 JST, 15 January 2001. On the other hand, the wind from the land developed at the lowest level from 0730 JST, 15 January 2001. The wind from the land at the lowest level developed in association with the decrease of the normal component to the coastline of the monsoon wind. After 1630 JST, 15 January 2001, the wind from the land kept its thickness of about 400 m. The wind direction at the lowest level was different from that of the sounding observed at Wajima. This indicates that a local wind, which was different from the monsoon wind, developed in the lowest layer in the area. The wind from the inland is referred to as the "land breeze," although the land breeze in the present case continued, not only in the nighttime, but also in the daytime. During the period of double bands, the land breeze steadily continued with almost constant thickness.

The horizontal extent of the land breeze over the land is shown using the AMeDAS wind data. Figure 11 shows the wind pattern at 2100
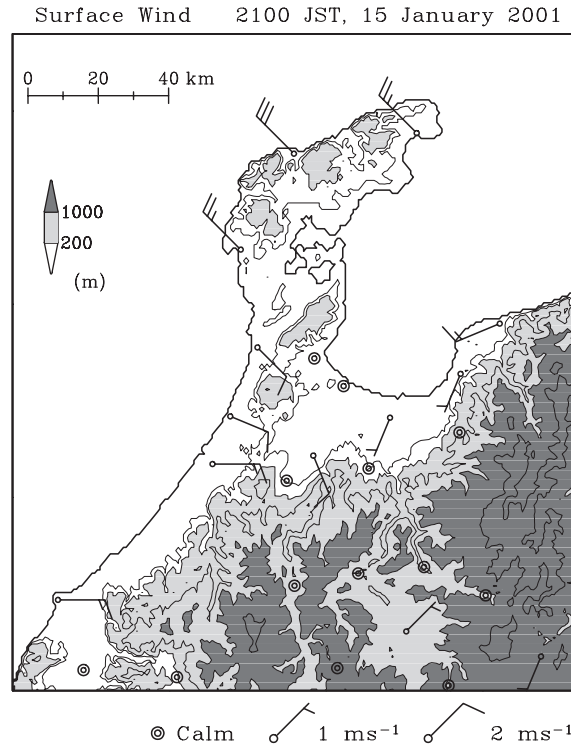
JST, 15 January 2001 during the period of double bands. In the northern part of the Noto Peninsula, the northwesterly monsoon wind was predominant. On the other hand, the land breeze locally extended in the coastal region of the Kanazawa Plain, the Tonami Plain, and the Toyama Plain. The easterly to southeasterly land breeze blew in the coastal region of the Kanazawa Plain.

The northwesterly monsoon wind, and the easterly to southeasterly land breeze, caused a convergence along the coast of the Kanazawa Plain. The location of the convergence zone is shown by time-averaged Doppler velocity at a height of 0.25 km, and reflectivity at a height of 0.5 km, obtained by the Oshimizu radar (Fig. 12). Positive Doppler velocity, which indicates the wind approaching the radar, was
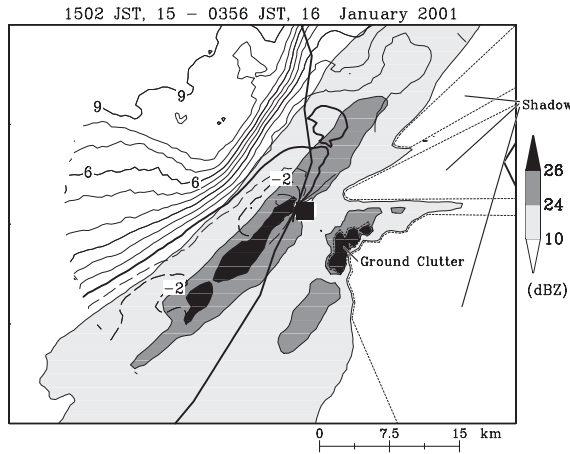
1502 JST, 15 – 0356 JST, 16   January 2001

Fig. 12. CAPPI display of the time-averaged Doppler velocity (contour lines, m s^{-1}) at a height of 0.25 km and time-averaged reflectivity (gray levels, dBZ) at a height of 0.5 km from 1502 JST, 15 to 0356 JST, 16 January 2001. The contours are drawn every 1 m s^{-1}. The positive Doppler velocity represents the wind approaching the Oshimizu radar marked with ■.
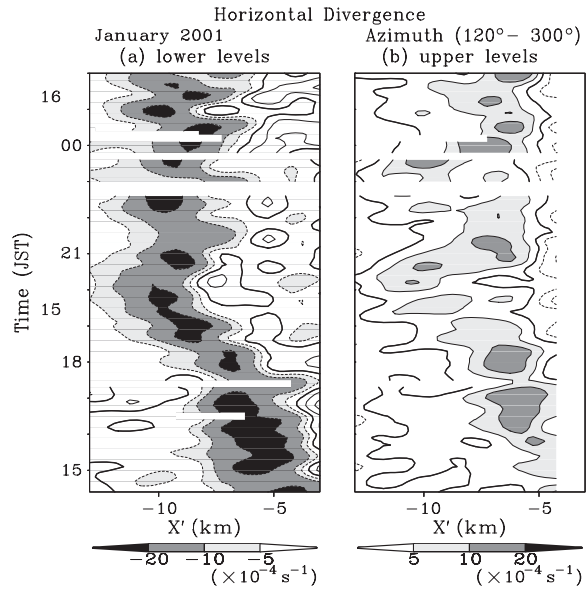

Fig. 13. Time-distance cross sections of the horizontal divergence in 10^{-4} s^{-1} derived from RHI scans of an orientation of 120° and 300°. (a) Lower levels (averaged for the height between 0.25 km and 0.75 km). (b) Upper levels (averaged for the height between 1.5 km and 2.0 km). The right-hand side of the figure is the landward side. The contours are drawn at −20, −10, −5, 0, 5, 10, and 20×10^{-4} s^{-1}.

widely present over the sea. This corresponds to the northwesterly monsoon wind. On the other hand, negative Doppler velocity, which indicates the wind away from the radar, was present on the landward side of the positive Doppler velocity. The maximum wind speed was 3 m s^{-1}. The negative Doppler velocity represents the land breeze. The crowded contours between the monsoon wind and the land breeze indicate the convergence zone. The convergence zone was parallel to the snowbands, and was located on the seaward side of Snowband 1 in the lower level.

Horizontal divergence along the land-breeze front is quantitatively estimated from the RHI data of an azimuth of 120°–300° during the period of double bands, where the X$'$ axis is defined as the distance toward an azimuth of 120° from the Oshimizu radar (Fig. 13). The orientation of the X$'$ axis is almost perpendicular to the snowbands. The right-hand side in the figure (toward the positive X$'$) is the landward side. Convergence of an order of 10^{-3} s^{-1} was present at almost the same position (X$'$ = −10 km to −5 km) throughout the period

of double bands in the lower levels (averaged for the height between 0.25 km and 0.75 km) (Fig. 13a). In the upper levels (averaged for the height between 1.5 km and 2.0 km), a continuous divergence of about 5×10^{-4} s^{-1} was present above the lower convergence zone (Fig. 13b). The convergence in the lower levels, and the divergence in the upper levels along the land-breeze front, indicate a steady updraft.

The relationship between the location of the cell and the land breeze is shown in Fig. 14. The contours with positive values indicate the monsoon wind, and those with negative values indicate the land breeze. The land-breeze front was located at X$'$ = −9 km. Above the land-breeze front, a new cell developed. On the landward side (the right-hand side in the figure) of the new cell, an old cell of Snowband 1 was present. On the farther inland side of the land-breeze front (around X$'$ = 5 km), the hori-
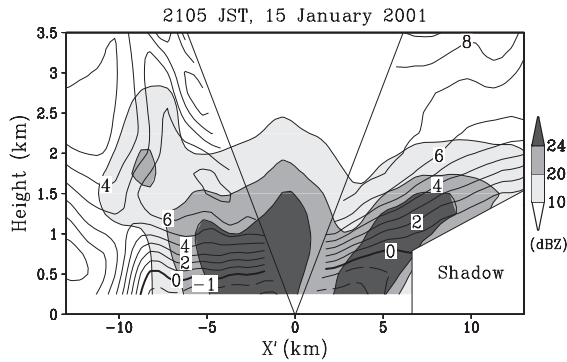
2105 JST, 15 January 2001

Fig. 14.   Vertical cross section of the reflectivity (gray levels, dBZ) and horizontal wind (contour lines, m s^{-1}) in the cross section derived from the RHI scan with an orientation of 120° and 300° at 2105 JST, 15 January 2001. The right-hand side of the figure is the landward side. The positive velocity indicates the wind blowing from the sea to the land.

zontal wind formed a weak convergence. A cell of Snowband 2 was located in this weak convergence zone. The echo pattern in Fig. 14 corresponds to the stage at 2102 JST, 2126 JST, and 2150 JST in Fig. 9.

Furthermore, the time-averaged features between the locations of the double snowbands and the airflow pattern are examined. Figures 15a and 15b show the time-averaged horizontal wind speed and the horizontal divergence in the cross section of the RHI scans, respectively. The horizontal wind speed was almost constant with height over the sea (around $X' = -30$ km) in the upwind side of the monsoon wind far from the snowbands. This horizontal wind significantly decreased in the lower level near the land-breeze front (between $X' = -14$ km and $X' = -4$ km below a height of 1.25 km). The zone in which the wind decreased corresponds to a convergence. The maximum convergence was -10^{-3} s^{-1} at $X' = -9$ km. The strong convergence in the lower level formed the strong updraft near the land-breeze front, which resulted in an upper-level divergence. The upper-level divergence was 4×10^{-4} s^{-1} ($X' = -8$ km) at a height of 2 km. The upper-level divergence zone corresponds to the region in which the horizontal wind increased in the X'-direction. On the other hand, the horizontal wind de-
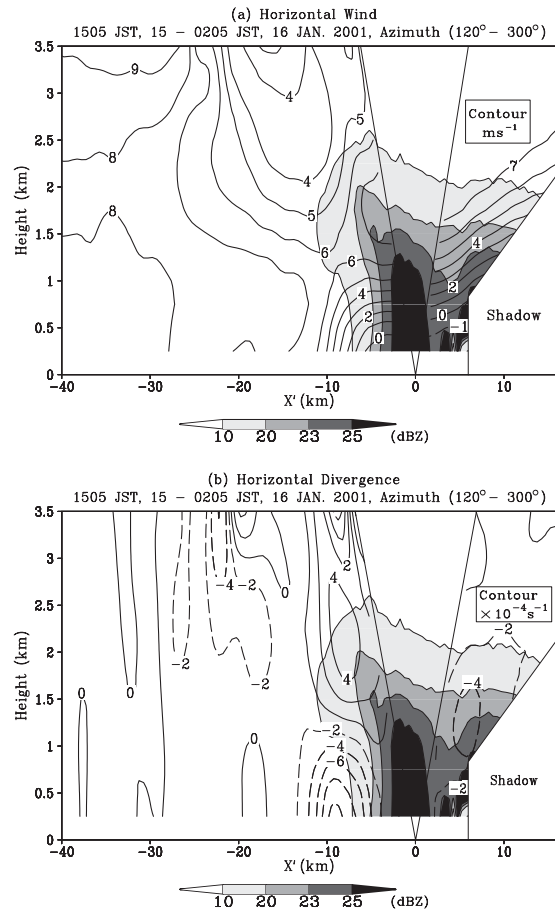

Fig. 15.   Vertical cross sections of (a) the horizontal wind (contour lines, m s^{-1}), (b) the horizontal divergence (contour lines, 10^{-4} s^{-1}) in the cross section, and the reflectivity (gray levels, dBZ) averaged from 1505 JST, 15 to 0205 JST, 16 January 2001 derived from the RHI scans with an orientation of 120° and 300°. The right-hand side in the figure is the landward side. The positive velocity indicates the wind blowing from the sea to the land.

creased in the X'-direction in the upwind side of the upper-level divergence zone. In the updraft region near the land-breeze front, reflectivity above 10 dBZ protruded toward the sea. This indicates that the updraft produced precipitation particles in the region. A new cell of Snowband 1, shown in Fig. 14, developed in this updraft region. In the inland side of the land-breeze front, the horizontal wind gradually decreased inside the contour of

the echo with 10 dBZ. This corresponds to a convergence. The maximum convergence was -4×10^{-4} s^{-1} at X$'$ = 5 km. The convergence indicates an updraft, because the convergence existed from the lowest level. The magnitude of the updraft in the inland side of the land-breeze front was smaller than that at the land-breeze front. Snowband 2 was located in the relatively weak updraft zone.

4.3 Cloud microphysical structure

The echo and airflow structures showed that the magnitude of reflectivity, the development speed of cells, and the magnitude of the updraft in Snowbands 1 and 2 were different. These differences suggest that the precipitation particle types, and their formation processes were different in the double snowbands. In this sub-section, the cloud microphysical aspects of the double snowbands will be described using dual-polarization radar data and pictures of snow particles. In the present case, the precipitation particles were only solid particles, because the surface temperatures of the AMeDAS points in the Kanazawa Plain were below the freezing point in the period of double bands. The re-flectivity in both bands (Figs. 5, 6, and 9) was not as strong as that in the case in which hail was present. Three solid precipitation particle types, namely, snow crystals, snow aggregates, and graupels are considered hereafter.

The distributions of Z and Z_{DR} derived from the Goishigamine radar are examined along the region where the echo cells were growing in each snowband. Transitions of the Z-Z_{DR} distributions along the trajectories reflect the growth of precipitation particles. The regions in which the transitions of Z-Z_{DR} are examined are selected in consideration of the time-averaged echo pattern and the movement of the echo cells. Figure 16b shows the time-averaged reflectivity pattern derived from the Goishig-amine radar during the period of double bands. The echo region in the seaward side from X = -8 km below a height of 0.75 km is sea clutter. The particles in Snowband 1 are in-ferred to move from Box 1 to 4 shown in Fig. 16b. On the other hand, the particles in Snow-band 2 are inferred to pass from Box 5 to 7.

The distributions between Z and Z_{DR} in each box in the period of double bands are presented in Fig. 16a. The rate in percentage shown in

the figure is calculated in the following manner. First, the number of grids included in a Z-Z_{DR} section is counted during the period of double bands, using the CAPPI data. The number of grids in the Z-Z_{DR} section is then divided by the number of all grids included in the box during the same period. For all Z-Z_{DR} sections, rates are calculated in the same manner.

In Box 1, which is concerned with Snowband 1, Z_{DR} data was scattered in a relatively wide range, which indicates particles with various shapes. The Z_{DR} data in Boxes 2, 3, and 4 was concentrated within the range of -0.25 dB to 0.5 dB, which indicates that spherical particles, including slightly vertically oriented particles, were present. Most of the Z data was con-centrated within the range of 19 dBZ to 25 dBZ in Box 4. This strong reflectivity and spherical feature including a slightly vertically oriented shape suggest that the dominant particles are graupels. Therefore, the transitions of Z and Z_{DR} from Box 2 to 4 indicate the development of spherical graupels, including conical ones, with almost no change of shape distribution.

In Box 5, which is concerned with Snowband 2, data of small Z and large Z_{DR} around 1 dB had a significant portion. Those data are thought to correspond to flat snow crystals. The portion of small Z and large Z_{DR} data decreased when moved from Box 5 to 7. Finally, in Box 7, Z and Z_{DR} data were concentrated on 16 dBZ to 22 dBZ, and 0 dB to 0.75 dB, respectively. The Z_{DR} between 0 dB and 0.75 dB indicates hori-zontally oriented particles. From their moder-ate reflectivity and horizontally oriented shape, the dominant particles in Snowband 2 are inferred to be snow aggregates. Consequently, the transitions of Z and Z_{DR} from Box 5 to 7 indicate the process through which the flat snow crystals were converted into snow aggregates.

Pictures of accumulated snow on the surface were taken at 1632 JST, 1724 JST, and 2231 JST, 15 January 2001 in the period of double bands at the Oshimizu radar site, which was located below Snowband 1. In those pictures, numerous graupels were found (not shown).

Below Snowband 2, 68 and 81 sheets of pic-tures of particles were taken at Hirakamachi and Yamada, respectively, between 2332 JST, 15 and 0343 JST, 16 January 2001 during the period of double bands. Only snow aggregates
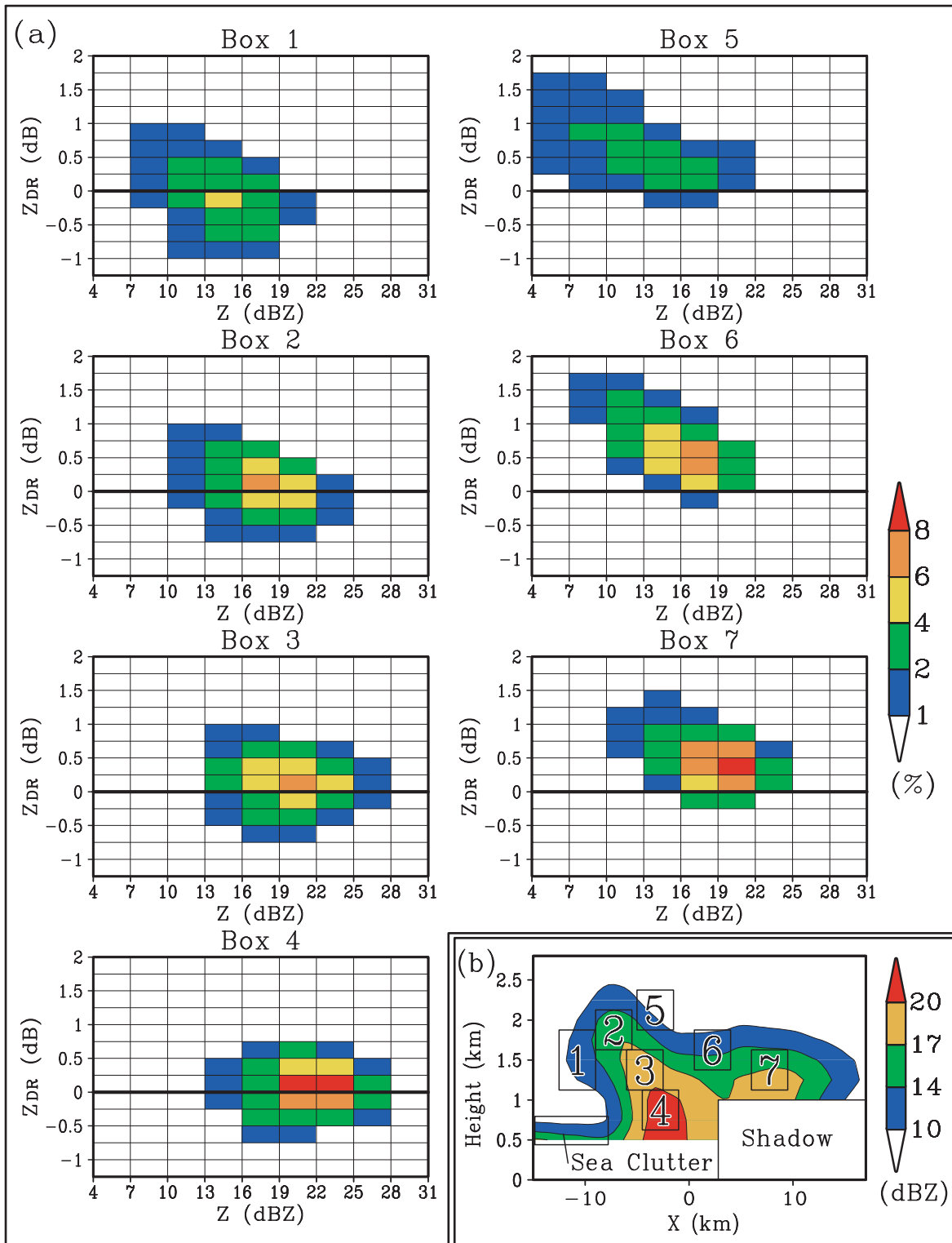
Fig. 16. *Z-Z$_{DR}$* distributions. (a) *Z-Z$_{DR}$* distributions in each box. The locations of the boxes are indicated by numbers in (b). The method used for the calculation of the rate is presented in the text. (b) Vertical cross section of the time-averaged reflectivity derived from the dual-polarization radar data averaged between Y = −24 km and −8 km (the rectangle area with broken lines in Fig. 5) from 1506 JST, 15 to 0356 JST, 16 January 2001. The contours are drawn at 10, 14, 17, and 20 dBZ.
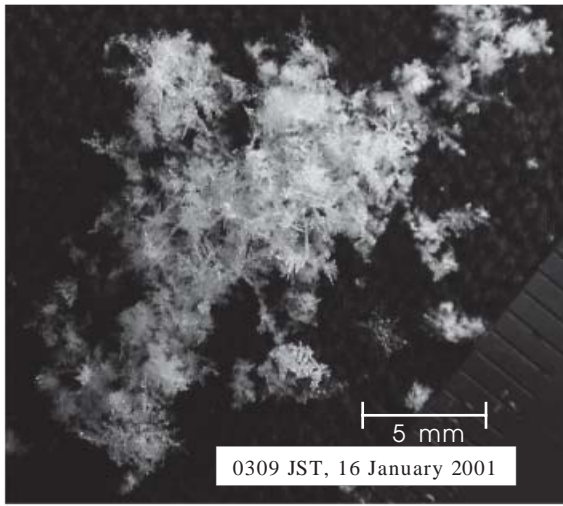
Fig. 17.　Picture of snow particles taken at 0309 JST, 16 January 2001 at Yamada.
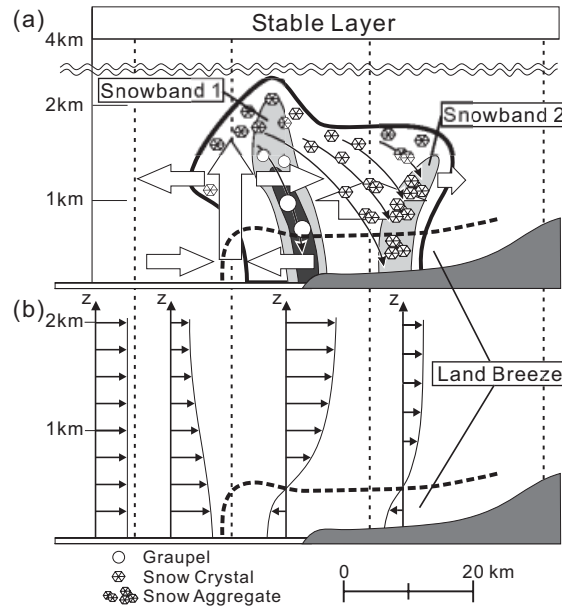

Fig. 18.　Schematic representation of the structures and maintenance processes of the double snowbands in the vertical cross section perpendicular to the alignment of the snowbands. The thick broken lines indicate the outline of land breeze. (a) The thick solid line represents the outline of the echo region. The strong reflectivity regions are shaded. The thick arrows show the wind relative to the ambient wind, and the thin arrows indicate the trajectories of particles. The precipitation particle types (graupel, snow crystal, and snow aggregate) are shown. (b) Vertical profiles of horizontal wind in the cross section.

were seen in the pictures. Figure 17 shows an example taken at 0309 JST, 16 January 2001 at Yamada. The snow aggregates were made up of heavily rimed crystals, and lightly rimed and unrimed crystals, such as dendrites.

The Z-Z_{DR} distributions in Snowbands 1 and 2, and the pictures of particles taken on the surface indicate that the main types of precipitation particles were graupels in Snowband 1, and snow aggregates in Snowband 2.

5.　Maintenance process of snowbands

The kinematical and microphysical processes of Snowbands 1 and 2 are discussed in this section. A schematic representation of the structures and maintenance processes of the double snowbands is given in Fig. 18. In the lower level of the mixing layer over the sea near Hokuriku, the northwesterly wind was predominant (Fig. 2). The wind speed (12 m s^{-1} at a height of 500 m at Wajima at 2100 JST, 15 January 2001) was moderate (Fig. 3). Furthermore, the pressure gradient from the sea to the land was weak at the surface level in the northeastern side of the JPCZ near the coastal region of Hokuriku (Fig. 2). The sea surface temperature around Hokuriku in January 2001 was between 12°C and 15°C, and the ground temperature was below 0°C, because snow covered the surface of the Kanazawa Plain. The

large temperature contrast between the land and sea produced a pressure gradient force from the land to the sea in the lower level. The pressure gradient force from the land to the sea caused the land breeze in the relatively weak ambient wind and pressure gradient from the sea to the land (Fig. 11). The above-mentioned conditions of the land and sea surfaces, and the ambient wind speed and pressure pattern in the lower level, did not vary significantly in the period of double bands. Therefore, the land breeze was maintained during the day and night in the period of double bands (Fig. 10).

The southeasterly land breeze caused a convergence with the northwesterly monsoon wind

along the coast (Fig. 12). Assuming that Snowband 1 had a 2-dimensionality, and that a convergence of 2×10^{-3} s^{-1} (Fig. 13) with a thickness of 1.25 km was present, an updraft of 2.5 m s^{-1} at a height of 1.25 km will be derived from the continuity equation under the Boussinesq approximation. The strong updraft caused a higher echo top of Snowband 1 (Figs. 8 and 9). It is expected that plenty of supercooled cloud water was produced in the strong updraft region. The particles with various shapes were present in the early stage of its formation in the strong updraft (Box 1 in Fig. 16a). When the particles became large, the riming process became effective in abundant supercooled cloud water. This resulted in the formation of graupels. The range of Z_{DR} with the maximum frequency (-0.25 dB to 0.5 dB) did not change significantly along the trajectory of the particles from Box 2 to 4. Therefore, spherical graupels, including conical ones, almost retained their shape through the riming process when the particles were falling relative to the ground. These processes provide an explanation for the stronger reflectivity that was observed in Snowband 1 (Figs. 6, 7, and 8).

The strong updraft along the land-breeze front resulted in the upper-level divergence (around -8 km in the X$'$-direction in Fig. 15b). In the upwind side of the upper-level divergence, the horizontal wind decreased (-27 km to -15 km in the X$'$-direction in Fig. 15a), while it increased in the downwind side (X$' > -10$ km). The increase and decrease of the horizontal wind are related to a high pressure. The location of the high pressure is explained below, using the 2-dimensional horizontal momentum equation. In this discussion, we consider a steady state in which a vertically constant mean wind blows, and ignore the Coriolis and the diffusion terms. Then, the linearized momentum equation is

$$\bar{u}\frac{\partial u'}{\partial x} = -\frac{1}{\rho_0}\frac{\partial p'}{\partial x}, \qquad (3)$$

where u, ρ_0, and p are the horizontal velocity, constant density, and pressure, respectively. The overbar denotes a mean component, and the primes represent deviation components. According to (3), a pressure maximum ($\partial p'/\partial x = 0$) is located along a zero divergence line ($\partial u'/\partial x = 0$), namely, a minimum wind speed line. This is a significant feature of the steady wind field. The pressure maximum balances with the decrease of the horizontal velocity in the upwind side, and the increase in the downwind side.

The horizontal velocity decreased in the further inland region, and formed a weak convergence (X$' > 0$ km in Figs. 15a and 15b), which is concerned with Snowband 2. The weak convergence corresponds to a relatively weak updraft. Three possible mechanisms responsible for the decrease in the horizontal wind speed, and the weak updraft will be discussed here. One possible mechanism is a vertical mixing of the horizontal momentum. Turbulent eddies in the atmosphere are likely to exchange the horizontal momentum in the strong vertical shear layer, between the land-breeze layer and its upper layer. This results in the deceleration of the monsoon wind over the land, and produces a weak updraft behind the land-breeze front. In the confined zone just behind the strong updraft of Snowband 1, a compensating downdraft is expected to be formed in the weak static stability. The reflectivity minimum between Snowband 1 and Snowband 2 was located at the expected compensating downdraft zone.

The second possibility causing the weak updraft is a gravity wave induced by steady heating. Lin and Li (1988) studied the response of a shear flow to a steady local heating using a linear theory. They explained the alternating upward and downward motions in the downstream of the heating region as the gravity wave response to steady heating. In Snowband 1 of our study, latent heat was released in the formation of cloud water and precipitation particles. The stationary Snowband 1 would produce steady heating. Thus, the vertical wind pattern shown in Lin and Li (1988, Fig. 2) is likely to be formed in the downstream. While no reflectivity maximums corresponding to the updrafts repeating in the downwind side shown in Lin and Li (1988) were observed, except for Snowbands 1 and 2, this process can explain the local reflectivity maximum of Snowband 2, as well as the reflectivity minimum between Snowbands 1 and 2.

The third proposed mechanism for the weak updraft is an updraft forced along the slope of topography. The slope of topography is present

in the inland side between 10 km and 15 km from the coastline in the Kanazawa Plain. The location of the slope almost corresponds to that of Snowband 2. Snowband 2 showed relatively strong reflectivity near Mt. Hodatsu (637 m), which is relatively high altitude (Figs. 1 and 7). This suggests that the topography was responsible for the intensification of the reflectivity of Snowband 2.

All three mechanisms mentioned above can contribute to the formation of the weak updraft associated with Snowband 2. To estimate each contribution quantitatively, however, further research using a numerical model will be required.

The main type of precipitation particles in Snowband 2 was snow aggregates, which included both rimed and unrimed crystals (Fig. 17). Some of the rimed and unrimed crystals were produced in Snowband 1, and were transferred to Snowband 2, because cellular echoes of Snowband 2 intensified in the weak echoes, which protruded from Snowband 1 toward Snowband 2. Unrimed crystals should also be produced and developed through the deposition process in the weak updraft in Snowband 2. However, the riming process is inferred to be ineffective in Snowband 2, because most cloud water was consumed in Snowband 1 in the upwind side of the monsoon wind, and the weak updraft in Snowband 2 did not produce so much cloud water. Figure 16 shows a decrease in the portion of the large Z_{DR} data, with weak reflectivity and the concentration of the Z_{DR} data around 0.5 dB, with strong reflectivity from Box 5 to 7. This indicates the conversion from flat snow crystals to snow aggregates through the aggregation process. The intensification of reflectivity in Snowband 2 was mainly caused by the aggregation process, which effectively produces large particles.

Although steady snowbands are the focus of this study, transient cells were shown in Fig. 9. Takeda et al. (1982) showed two intensification stages of isolated convective cells of snow clouds along a coast. If some cells, such as those shown in Takeda et al. (1982), form double bands, the double-band structure can be seen in a time-averaged pattern. However, its structure will be hardly seen in a snapshot, because cells have various stages. This is inconsistent with the fact that the double snowbands were

seen in the snapshot of Fig. 5, and indicates that a steady structure maintaining the double bands was present in our case. The generations and dissipations of cells are a transient part superposed on the steady structure and not essential for the steady double-band structure. While Tsuboki et al. (1989b) showed successive intensifications of snowband echoes at a stationary land-breeze front, the double-band structure did not appear. In their case, a convective snowband came into the stationary land-breeze front and was intensified. It is inferred that substantial updrafts were present in the snowband approaching the land-breeze front, because the snowband showed significant reflectivity. Circulation with the significant updrafts within the snowband can be predominant, and interact with the circulation around the land-breeze front, to bring a type of circulation different from that in our case. Before the period of double bands in the present case, convective echoes that developed over the sea frequently merged into the snowbands formed along the land-breeze front, and the double-band structure was unclear (Fig. 6). This is similar to the case shown by Tsuboki et al. (1989b). These facts indicate that the steady structure formed around the land-breeze front without interactions with merged precipitating snow clouds, was essential for the maintenance of the double snowbands.

6. Summary

When a cold air outbreak occurred in the middle of January 2001, double snowbands stayed along the coastal region, from 15 to 16 January in Hokuriku. The kinematical and cloud microphysical structures of the stationary double snowbands were studied, mainly using Doppler and dual-polarization radars, to clarify the intensification processes of snowfall in the coastal region. Their maintenance processes were discussed.

The double snowbands, which are referred to as "Snowband 1" and "Snowband 2," stayed along the coast for about 20 hours. The separation of double snowbands gradually became clear with time. We focused on the period in which the separation of double snowbands was clear. The period is referred to as the "period of double bands." Snowband 1 was present on the seaward side, with relatively strong reflectivity,

and a higher echo top. On the other hand, Snowband 2 was located at the landward side, and had relatively weak reflectivity. The echo top of Snowband 2 was relatively lower. The sequential echo pattern showed that a new echo cell in Snowband 2 developed in the weak echo region, which extended from Snowband 1 toward Snowband 2 after a strong echo cell in Snowband 1 descended.

Airflow patterns around the snowbands showed that an easterly, or a southeasterly land breeze was present over the Kanazawa Plain. The local wind, which flows from the land to the sea, is referred to as a "land breeze" in this study. The land breeze developed from the morning of 15 January, and had a thickness of about 400 m above the Oshimizu radar in the period of double bands. It caused a convergence with the northwesterly monsoon wind in the lower level on the seaward side of Snowband 1. The convergence reached -2×10^{-3} s^{-1}. In the upper level above the convergence zone, between the monsoon wind and the land breeze, a divergence of 10^{-3} s^{-1} was present. The convergence in the lower level and the divergence in the upper level correspond to a strong updraft. This strong updraft produced Snowband 1. On the other hand, a weak convergence zone was also present in Snowband 2. The weak convergence corresponds to a weak updraft.

The difference in the cloud microphysical process for the formation of Snowbands 1 and 2 was also examined. The strong updraft in Snowband 1 formed graupels through the riming process. On the other hand, a weak updraft in Snowband 2 promoted the deposition process. The riming process was considered to be ineffective in Snowband 2, because the amount of cloud water was poor in the weak updraft. The sequential echo patterns demonstrate that some crystals formed in Snowband 1, flowed toward Snowband 2. The snow crystals generated in both snowbands contributed to the formation of the snow aggregates in Snowband 2 through the aggregation process.

Acknowledgments

References

Asai, T., 1988: Meso-scale features of heavy snowfalls in Japan Sea coastal regions of Japan. *Tenki*, **35**, 156–161 (in Japanese).

Fujiyoshi, Y., K. Tsuboki, H. Konishi, and G. Wakahama, 1988: Doppler radar observation of convergence band cloud formed on the west coast of Hokkaido Island (I)—Warm fontal type—. *Tenki*, **35**, 427–439 (in Japanese).

Gal-Chen, T., 1982: Errors in fixed and moving frame of references: Applications for conventional and Doppler radar analysis. *J. Atmos. Sci.*, **39**, 2279–2300.

Harimaya, T. and N. Kanemura, 1995: Comparison of the riming growth of snow particles between coastal and inland area. *J. Meteor. Soc. Japan*, **73**, 25–36.

——— and M. Sato, 1992: The riming proportion in snow particles falling on coastal areas. *J. Meteor. Soc. Japan*, **70**, 57–65.

Ishihara, M., H. Sakakibara, and Z. Yanagisawa, 1989: Doppler radar analysis of the structure

of mesoscale snow bands developed between the winter monsoon and the land breeze. *J. Meteor. Soc. Japan*, **67**, 503–520.

Lin, Y.-L. and S. Li, 1988: Three-dimensional response of a shear flow to elevated heating. *J. Atmos. Sci.*, **45**, 2987–3002.

Passarelli, R.E., Jr. and R.R. Braham, Jr., 1981: The role of the winter land breeze in the formation of Great Lake snow storms. *Bull. Amer. Meteor. Soc.*, **62**, 482–491.

Seliga, T.A. and V.N. Bringi, 1976: Potential use of radar differential reflectivity measurements at orthogonal polarizations for measuring precipitation. *J. Appl. Meteor.*, **15**, 69–76.

Takeda, T., K. Isono, M. Wada, Y. Ishizaka, K. Okada, Y. Fujiyoshi, M. Maruyama, Y. Izawa, and K. Nagaya, 1982: Modification of convective snow-clouds in landing the Japan Sea coastal region. *J. Meteor. Soc. Japan*, **60**, 967–977.

Tsuboki, K. and G. Wakahama, 1988: Single Doppler radar measurements of a kinematic wind field: VAD analysis based on a least-squares-fitting method. *Low Temperature Science*, **47**, 73–88 (in Japanese with English summary).

——, Y. Fujiyoshi, and G. Wakahama, 1989a: Doppler radar observation of convergence band cloud formed on the west coast of Hokkaido Island. II: Cold frontal type. *J. Meteor. Soc. Japan*, **67**, 985–999.

——, ——, and ——, 1989b: Structure of a land breeze and snowfall enhancement at the leading edge. *J. Meteor. Soc. Japan*, **67**, 757–770.

Yoshizaki, M., T. Kato, H. Eito, A. Adachi, M. Murakami, S. Hayashi, and WMO-01 observation group, 2001: A report on "Winter MCSs (mesoscale convective systems) Observation over the Japan Sea in January 2001 (WMO-01)". *Tenki*, **48**, 893–903 (in Japanese).